crystals

MDPI

Article

Microstructures and Mechanical Properties of Nanocrystalline AZ31 Magnesium Alloy Powders with Submicron TiB_2 Additions Prepared by Mechanical Milling

Haiping Zhou [1], Chengcai Zhang [1], Baokun Han [1], Jianfeng Qiu [2], Shengxue Qin [1], Kuidong Gao [1], Jie Liu [1], Shuai Sun [1] and Hongbin Zhang [1,*]

[1] College of Mechanical and Electronic Engineering, Shandong University of Science and Technology, Qingdao 266590, China; zhouhp@sdust.edu.cn (H.Z.); skd996028@sdust.edu.cn (C.Z.); skd990444@sdust.edu.cn (B.H.); skd992892@sdust.edu.cn (S.Q.); gaokuidong@sdust.edu.cn (K.G.); skd993978@sdust.edu.cn (J.L.); skd996026@sdust.edu.cn (S.S.)

[2] Medical engineering and technology center, Shandong First Medical University & Shandong Academy of Medical Sciences, Taian 271000, China; jfqiu100@gmail.com

* Correspondence: zhanghb@sdust.edu.cn

Received: 26 May 2020; Accepted: 25 June 2020; Published: 26 June 2020

Abstract: In this work, nanocrystalline AZ31 magnesium alloy powders, reinforced by submicron TiB_2 particles, were prepared via mechanical milling. It was found that TiB_2 particles stimulated the fracture and welding of AZ31/TiB_2 powders, leading to the acceleration of the milling process. Meanwhile, the TiB_2 particles were refined to submicron-scale size during the milling process, and their distribution was uniform in the Mg matrix. In addition, the matrix was significantly refined during the milling process, which was also accelerated by the TiB_2 particles. The formation of grain boundary segregation layers also led to the weakened TiB_2 peaks in the XRD patterns during the mechanical milling. The grain sizes of AZ31–2.5 wt % TiB_2, AZ31–5 wt % TiB_2 and AZ31–10 wt % TiB_2 powders were refined to 53 nm, 37 nm and 23 nm, respectively, after milling for 110 h. Under the combined effect of the nanocrystalline matrix and the well-dispersed submicron TiB_2 particles, the AZ31/TiB_2 composites exhibited excellent micro-hardness. For the AZ31–10 wt % TiB_2 composite, the micro-hardness was enhanced to 153 HV0.5.

Keywords: mechanical milling; magnesium powder; TiB_2 particles; nanocrystalline; mechanical properties

1. Introduction

At present, the development of high-strength light alloys has been required to meet the light-weight requirements, which is of great significance for energy saving in structural applications [1]. As the lightest structural metallic materials, magnesium (Mg) alloys have favorable application prospects in the fields of aerospace, automobile, electronics and other industries, because of their low density, high specific stiffness and strength, and good shock absorption [2,3]. However, the technical challenge in the wide application of Mg alloys was their low mechanical properties, especially at elevated temperatures (>200 °C) [4–6]. In order to extend the structural application of Mg alloys, it is necessary to search for effective methods to further strengthen the commercial Mg alloys.

It is widely proposed that grain refinement is an important method of strengthening metallic materials, while the nanocrystalline (NC) and ultrafine-grained (UFG) materials can exhibit better mechanical properties when compared with conventional coarse-grained materials [7,8]. For Mg alloys,

NC and UFG microstructures are extremely tempting, owing to the high Hall–Petch coefficient (k_y) [9]. For instance, Feng et al. [2] proposed that when the grain size of the Mg-3Al-Zn alloy was refined to only 246 nm, the increasing yield stress of the alloy could reach about 119.78 MPa due to grain refinement. In addition, the grain refinement of Mg alloys has been realized via various methods, including high pressure torsion (HPT) [10], accumulative roll bonding (ARB) [11], equal channel angular extrusion (ECAE) [12], friction stir processing (FSP) [13], mechanical milling (MM) [6,14], etc. Among them, MM has been considered to be an available method for preparing NC Mg alloys [15]. Fang et al. [14] successfully prepared NC Mg-3Al-Zn alloy powders via ball milling, and their average grain size was refined to 45 nm. Yu et al. [6] prepared NC AZ61–10 at.% Ti alloy powders by MM, the micro-hardness of which could reach 120 HV.

Simultaneously, the addition of particle reinforcements, such as SiC particles [16], B_4C [17], Al_2O_3 particles [18] and AlN [19] particles, was another effective approach to strengthening Mg alloys. Matin et al. [16] successfully fabricated AZ80/SiC nano-composites via the stir casting method, and their hardness value increased from 49 to 59 HV when the SiC content increased from 0% to 3.5%. Aydin et al. [17] prepared Mg/B_4C composites via powder metallurgy, while the increments on compressive yield strength and hardness reached about 69.5% and 63.9%, for 30 wt % B_4C, as compared to pure Mg. Rahmany-Gorji et al. [20] studied the influence of Al_2O_3 micro-particles on the properties of ZX51 alloy; the hardness of ZX51/Al_2O_3 composites increased to 72.0 HB, while the hardness was only 58.1 HB for ZX51 alloy. Sankaranarayanan et al. [19] reported that the strength of pure Mg was effectively improved by the nano-AlN particulates.

In addition, the TiB_2 particle was another favorable reinforcer of the Mg matrix composite, owing to its high modulus, low density and low cost [21]. In particular, the crystal structures of both TiB_2 and Mg are close-packed and hexagonal [21–23], and the coherent lattice relationships could be formed at their interface. At present, TiB_2 particle reinforcement has received increasing attention with regards to Mg matrix composites. Wang et al. [22] studied the influence of fine TiB_2 (~7 μm) particles on the mechanical properties of AZ91 alloy, and the hardness of AZ91/TiB_2 composites increased by 20 HB with 7.5 wt % TiB_2 particles. Aydin et al. [23] studied the properties of hot-pressed TiB_2 particulate-reinforced Mg matrix composites, and their hardness increment was 65.3% with 30 wt % TiB_2 particles, as compared to pure Mg. At present, investigations into Mg/TiB_2 composites are still rather limited, and more works should be carried out to realize the great potential of TiB_2 additions in Mg matrix composites.

In this study, the NC AZ31/TiB_2 Mg matrix composites were fabricated by mechanical milling. Meanwhile, the evolution of microstructures, including powder morphology, the dispersion of TiB_2 particles in the matrix and Mg grain, was investigated during mechanical milling. Moreover, the properties and strengthening mechanism of the composites were analyzed in detail.

2. Experimental Procedures

The as-cast AZ31 Mg alloy (Al 3.06 wt %, Zn 1.01 wt %, Mn 0.3 wt %, Si 0.028 wt %, Cu 0.0022 wt %, Fe 0.0015 wt %, Ni 0.00046 wt %, Mg Bal.) and TiB_2 with particle sizes of 3 μm (99.9%, Ti 68.83 wt %, B 31.07 wt %, O 0.07 wt %, C 0.02 wt %, Fe 0.01 wt %) were used as the initial materials, and the AZ31 Mg alloy ingot was mechanically cut into chips with a thickness of about 0.2 mm. The AZ31 Mg alloy and TiB_2 particles were purchased from RSR company, and Jonyetch ceramic Ceramic Technology company in China, respectively. Figure 1 shows the morphology of the AZ31 Mg alloy chips and TiB_2 particles. It can be found that the AZ31 Mg alloy chips exhibited laminar morphology, and TiB_2 particles exhibited polygonal morphology. Figure 2 shows the XRD patterns of initial AZ31 Mg alloy and TiB_2 particles. From the XRD results, it can be seen that the Mg and TiB_2 phases were detected clearly, and no other phases were detected. In addition, all the materials were weighed and mixed in a glove box filled with high purity argon (99.9%), in order to avoid oxidation.

Before mechanical milling, the AZ31 chips and TiB_2 particles were mixed together with different TiB_2 particle additions of 2.5 wt %, 5 wt % and 10 wt %, while each mixture was 10 g in weight. Then, the mixtures and stainless-steel balls (ϕ 5 mm, ϕ 8 mm, ϕ 10 mm) were put into the milling pots,

which were also filled with inert argon gas. The mechanical milling was executed by a QM-3SP4 type planetary ball milling machine (Nanjing NanDa Instrument Plant, Nanjing, China). Through the preparation experiment, the optimum milling parameters were determined, which were given as follows: the mass ratio of ball to powder was 60:1 and the shaft rotation was 300 rpm. Then, the AZ31/TiB_2 composite powders were cold pressed into green compacts (Φ 10 mm) under pressure of 1500 MPa, in the atmosphere of high purity argon (99.9%). Moreover, the relative densities of those green compacts could reach above 95%, which were calculated through the Archimedes method. The micro-hardness of the green compacts was measured using an HVS-1000 tester (Shanghai Optical Instrument Factory, Shanghai, China), with the load of 500 g and loading time of 20 s. The green compacts were carefully polished before hardness measurements.

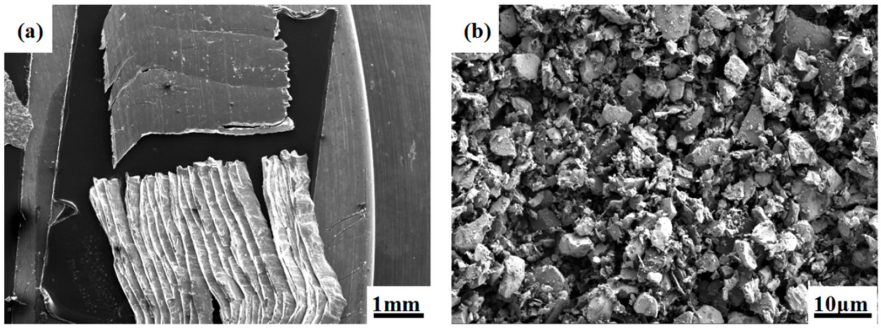

Figure 1. The morphology of initial materials: (**a**) AZ31 Mg alloy chips and (**b**) TiB_2 particles.

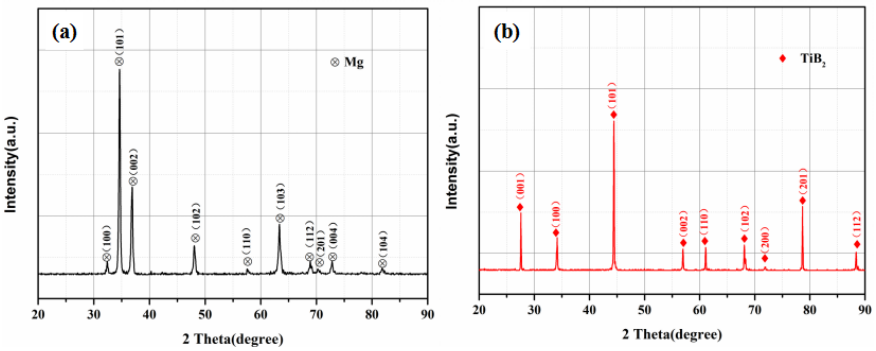

Figure 2. The XRD patterns of initial materials: (**a**) AZ31 Mg alloy chips and (**b**) TiB_2 particles.

In addition, X-ray diffraction (XRD, Rigaku Utima IV, Rigaku corperation, Japan) was utilized to examine the as-milled composite powers, using Cu-Kα radiation (40 Kv, 40 mA). According to the XRD results, the grain size of the matrix was calculated using Scherrer's equation [24]. In this study, the as-milled powders were directly used as scanning electron microscope (SEM) samples, which were observed using a FEI APREO scanning electron microscope (FEI Company, Hillsboro, USA). The samples for SEM observation were prepared in the glove box filled with high purity argon (99.9%) and kept in the sealed sample boxes. The back scattered electron (BSE) images were used to analyze the distribution of TiB_2 particles in the matrix. Meanwhile, a JEM-200 EX transmission electron microscope (TEM, JEOL Ltd, Tokyo, Japan) was utilized to identify the grain size of the as-milled AZ31 Mg alloy with different TiB_2 additions. The samples for TEM analysis were mechanically ground first, and polished to the thickness of 50 μm. Then, the polished TEM films were prepared using ion mill polishing.

3. Results and Discussion

3.1. Morphology Evolution of Powders

It is widely proposed that the MM process consists of repeated plastic deformation, cold welding and the fracturing of mixed powders through high-energy impact [25]. Meanwhile, the mechanical

milling has significant influence on the particle size and particle shape of the as-milled powders. Figure 3 shows the morphological evolution of the composite powders, with a 5 wt % TiB_2 addition after milling for different times. From Figure 3a,b, it can be observed that many laminar powders were fractured from the AZ31 Mg alloy cutting chips. Meanwhile, it can also be observed that some laminar powders piled up, which was mainly attributed to the cold welding during the milling process. In other words, there was a competitive relationship between the fracture and welding of these powers. As the milling time was prolonged, the fracture mechanism became predominant, resulting in the decrease of particle size. After milling for 60 h, it can be seen that many particles were changed into a rod shape, as shown in Figure 3f. In addition, the length to width radio of particle size decreased gradually during the milling process, as shown in Figure 3c–k. Yu et al. [6] also reported a similar phenomenon for AZ61/Ti composite powders during mechanical milling. Such a phenomenon was the result of the severe plastic deformation of powders in the process of mechanical milling, induced by the high-speed impact of stainless-steel balls in the rotating milling pots [25]. After milling for 100 h, there was no significant change in the particle size, which reached a stable stage, as shown in Figure 3j–k. Meanwhile, the average particle size was refined to about 700 μm after milling for 110 h, and many particles became equiaxed. It should be noted that the particles with larger volume and higher hardness were prone to fracture, which was beneficial to equiaxation of the particles' shape [26]. Besides that, the occurrence of cold welding could also contribute to the appearance of equiaxed particles. It is widely proposed that the interfacial energy of powders would increase sharply with the emergence of a large number of small particles [27], which could promote the welding of powders.

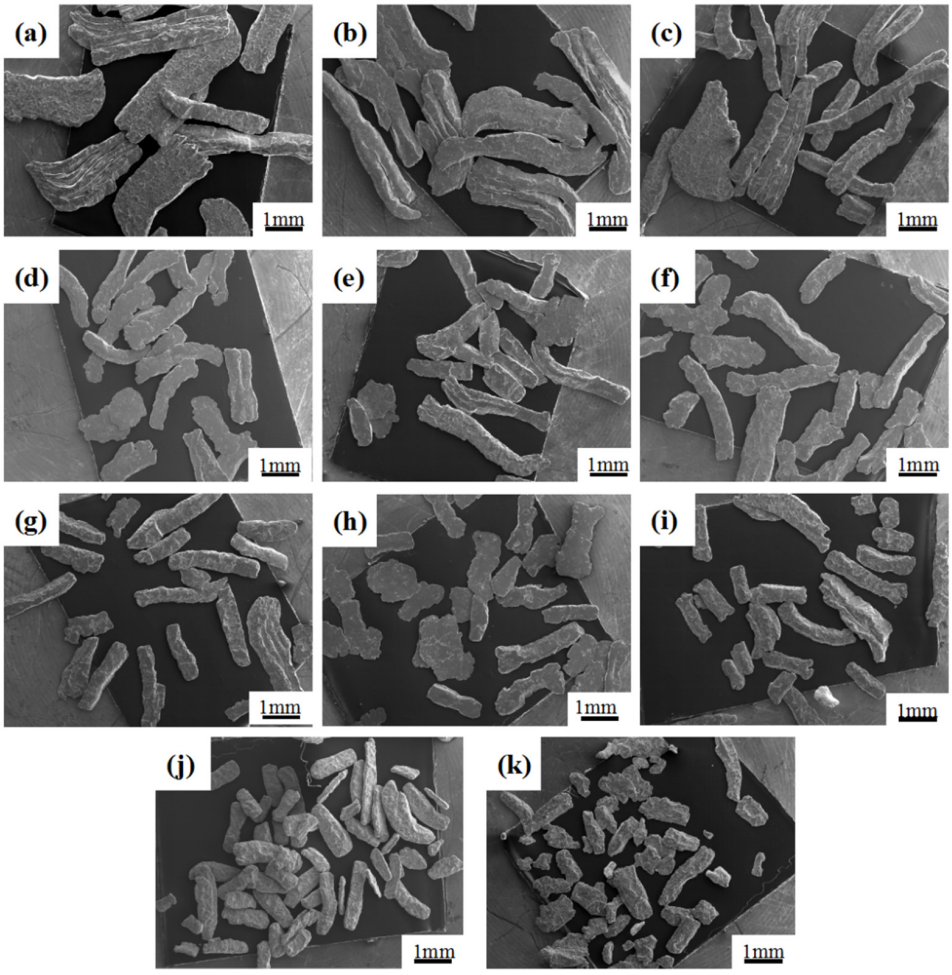

Figure 3. Morphologies of composite powders with 5 wt % TiB_2 addition after different milling times: (**a**) 10 h, (**b**) 20 h, (**c**) 30 h, (**d**) 40 h, (**e**) 50 h, (**f**) 60 h, (**g**) 70 h, (**h**) 80 h, (**i**) 90 h, (**j**) 100 h, (**k**) 110 h.

As shown in Figure 4, the content of the TiB_2 additions also has a great influence on the morphologies of the powders. Combining Figure 3c,g,k and Figure 4, it can be found that both the length to width ratio and particle sizes decreased with the increasing content of TiB_2 additions, and there were more equiaxed particles in the composite powders with high TiB_2 additions. In other words, the presence of hard TiB_2 additions could promote the fracturing of matrix particles, and accelerate the milling process, and they therefore acted as milling assistant agents. Meanwhile, the high stress concentration appeared as TiB_2 particles embedded in the matrix, which would promote the fracture of powders. Meanwhile, the reinforcement particles with high hardness significantly enhanced the local deformation of the matrix [28]. It can be inferred that the enhanced deformation caused by TiB_2 particles would stimulate the cold welding and fracture of powders, leading to the acceleration of the milling process.

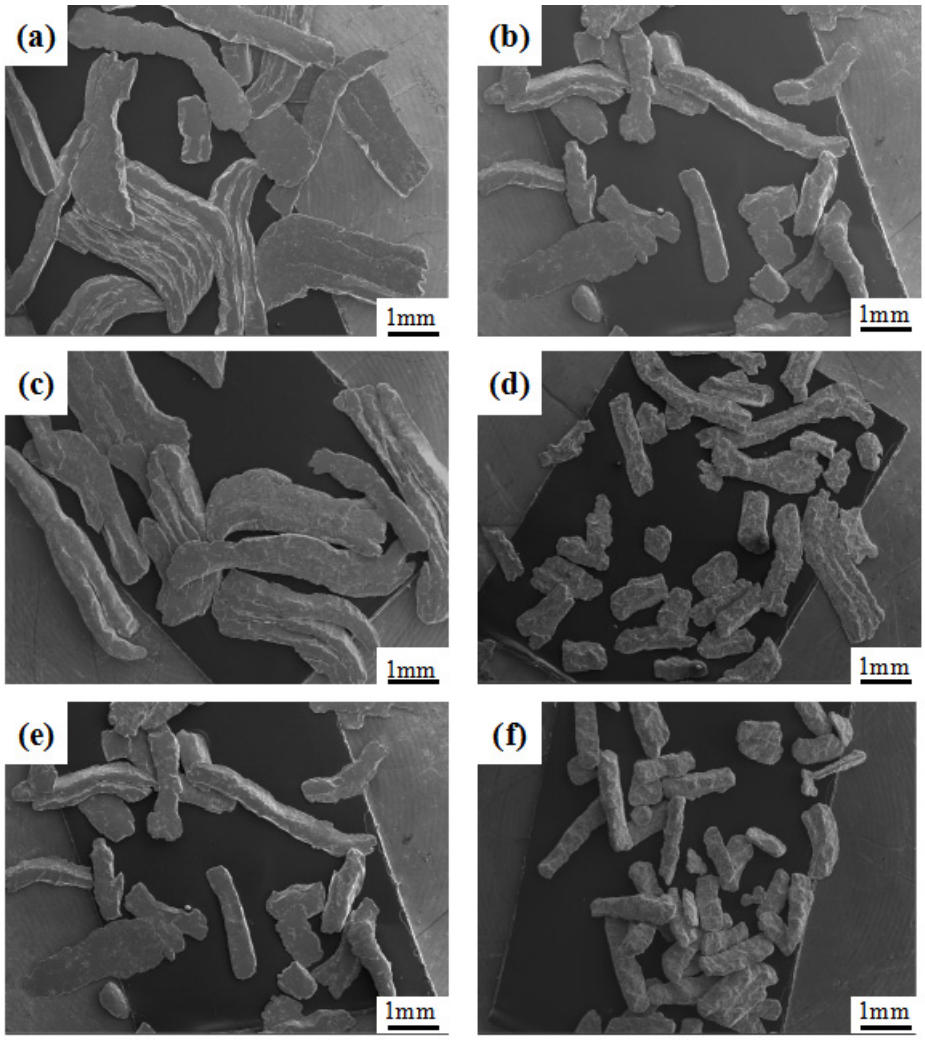

Figure 4. Morphologies of composite powders with different TiB_2 additions after milling for 30 h, 70 h and 110 h: (**a**) 30 h, 2.5 wt %, (**b**) 30 h, 10 wt %, (**c**) 70 h, 2.5 wt %, (**d**) 70 h, 10 wt %, (**e**) 110 h, 2.5 wt %, (**f**) 110 h, 10 wt %.

3.2. *Evolution of TiB_2 Particles*

As mentioned above, the TiB_2 reinforcement has a positive effect on the refinement rate of powders during mechanical milling. Moreover, the characteristics of TiB_2 particles are also very important for the properties of the composite materials, including the size of TiB_2 particles and their distribution in matrix [29]. To investigate the evolution of TiB_2 particles during mechanical milling, the BSE images

of the AZ31/TiB_2 powders were analyzed in detail. These images were taken from the flat parts in powders. Figure 5a–f shows BSE images of AZ31/TiB_2 powders with 5 wt % TiB_2 addition after milling for different times. Meanwhile, the EDS results of point A and point B marked in Figure 5a were also given, as shown in Figure 5g–h. According to the EDS result of point A, the gray area in the BSE images was identified as AZ31Mg alloy. As for the EDS result of point B, there were Ti and B elements in the white particles, which were the components of TiB_2. In other words, the white particles should be the TiB_2 additions.

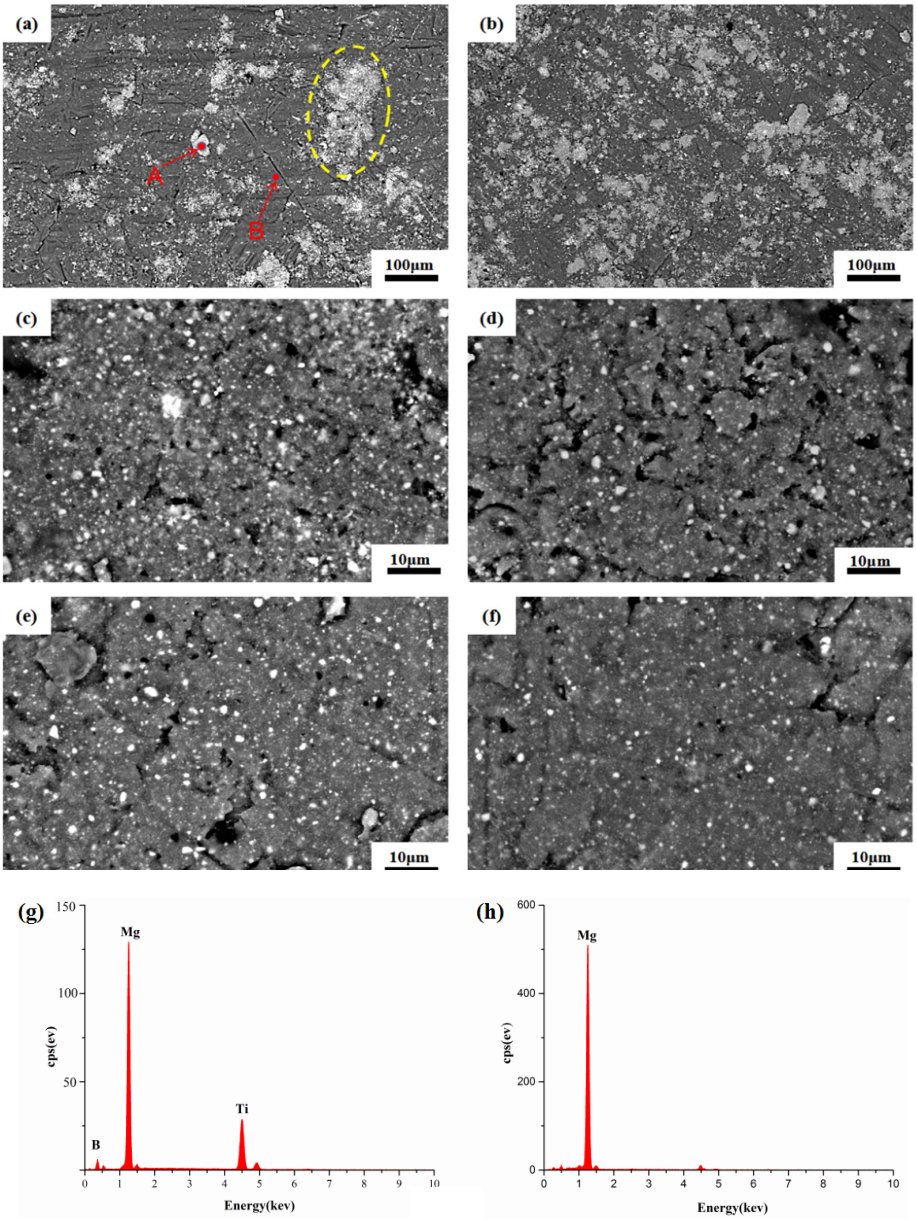

Figure 5. The BSE images of composite powders with 5 wt % TiB_2 addition after milling for different times, and the corresponding EDS results: (**a**) 10 h, (**b**) 30 h, (**c**) 50 h, (**d**) 70 h,(**e**) 90 h, (**f**) 110 h, (**g**) EDS results of point A, (**h**) EDS results of point B.

After milling for 10 h, a high quantity of TiB_2 particles assembled on the surface of matrix, and the distribution of TiB_2 particles exhibited a reunited state. As in Figure 5a, there was a typically large cluster, marked with the yellow ellipse region, which was mainly composed of TiB_2 particles. The formation of this large cluster was mainly caused by the inadequate milling. With the increasing

milling time, cold welding and deformation occurred in the Mg matrix. In this case, these clusters between two or more matrix particles would be wrapped in the matrix at the instant of ball-collision, leading to the dispersion of clusters in the matrix. As shown in Figure 5b, there were also TiB_2 clusters after milling for 30 h, due to the existence of an agglomeration force between TiB_2 particles. Meanwhile, these TiB_2 clusters would also be gradually disintegrated by the high-energy collisions between the grinding balls and powders. After milling for 50 h, it can be observed that there were few clusters of TiB_2 particles in matrix, as shown in Figure 5c, and the distribution of TiB_2 particles was uniform. With the increase in milling time, it is interesting to find that there were some big TiB_2 particles around the crack, while the fine TiB_2 particles uniformly dispersed in the Mg matrix, as shown in Figure 5d–f. In other words, the dispersed fine particles were easily entered into the matrix, which can promote the uniform distribution of reinforcing particles. Meanwhile, the big TiB_2 particles seemed to be more tended towards promoting the fracture of the Mg matrix, due to the introduction of a high stress concentration. From Figure 5c–f, it can also be seen that the average size of the TiB_2 particles was refined with the prolonging of milling time. The refinement of TiB_2 particles was mainly attributed to the fracture mechanism, which was similar to the refinement of the matrix. Then, an increasing number of fine particles entered into the matrix, and the uniform distribution of TiB_2 particles in the Mg matrix was gradually achieved. After milling for 110 h, the average size of TiB_2 particles was refined to about 0.4 μm, which had reached submicron-scale. As reported, the homogeneous distribution of submicron-scale TiB_2 particles could noticeably strengthen the matrix through the Orowan strengthening mechanism [30]. Besides that, not only was the size of TiB_2 particles refined during mechanical milling, but the sharp edges of the TiB_2 particles were also gradually eliminated, leading to a rounder morphology.

Based on the BSE images, it was found that 5 wt % TiB_2 particles of uniform size were uniformly distributed in the matrix after milling for 110 h. In order to further confirm the distribution at the element scale, the EDS maps of Mg, Ti, Al, Mn and Zn were characterized, as shown in Figure 6. It should be noted that all the Ti element in the EDS maps existed in the TiB_2 particles, which can be confirmed by the XRD analysis shown in Section 3.3. After milling for 110 h, the Ti element was uniformly distributed in the Mg matrix, as shown in Figure 6c, indicating the uniform distribution of TiB_2 particles. From Figure 6d–f, it can be observed that most of the Al, Mn and Zn elements were homogeneously dissolved into the Mg matrix. However, there were also some Al element existing in the $Mg_{17}Al_{12}$ phase, and there were also intermetallic compounds or solid solutions of Mn in the matrix after milling for 110 h, which are highlighted by the ellipse regions.

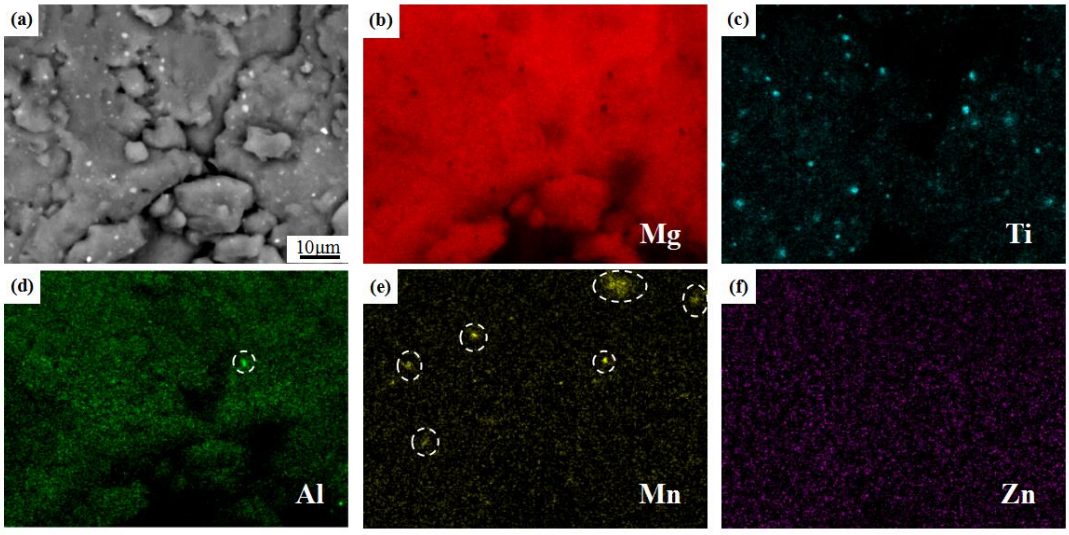

Figure 6. The SEM image (**a**) and corresponding EDS maps of Mg (**b**), Ti (**c**), Al (**d**), Mn (**e**) and Zn (**f**) for the composite powders with 5 wt % TiB_2 addition after milling for 110 h.

3.3. XRD Analysis

Figure 7 shows the XRD patterns of AZ31/TiB_2 composite powders with different TiB_2 additions after milling for different times. According to the result of XRD, the appearance of Mg and TiB_2 peaks can be clearly observed. However, it was very difficult to find $Mg_{17}Al_{12}$ peaks in the XRD patterns of the AZ31/TiB_2 composite powders after mechanical milling, which was very similar to the other investigations [6,31]. Such a phenomenon was mainly owing to the decomposition of the $Mg_{17}Al_{12}$ phase and the dissolving of Al into the Mg matrix during the milling process [31]. In addition, there were no other new phases detected in the XRD patterns after milling for different times, indicating that the TiB_2 particles did not react with the matrix during the milling process. Simultaneously, the diffraction intensity of the Mg peaks decreased with the increasing milling time, while the full width was attained at half the maximum of the Mg peaks' increase. Such a phenomenon was closely related to the refinement of grain size [24]. Meanwhile, the grain size can be approximated from the XRD data by using the following formula [24]:

$$D = \frac{k\lambda}{\beta_C^f \cos\theta} \tag{1}$$

where D is the grain size, k is the Scherrer constant, λ is the wavelength of the radiation, θ is the Bragg angle, and β_C^f can be calculated from the ratio of the Cauchy integral's breadth.

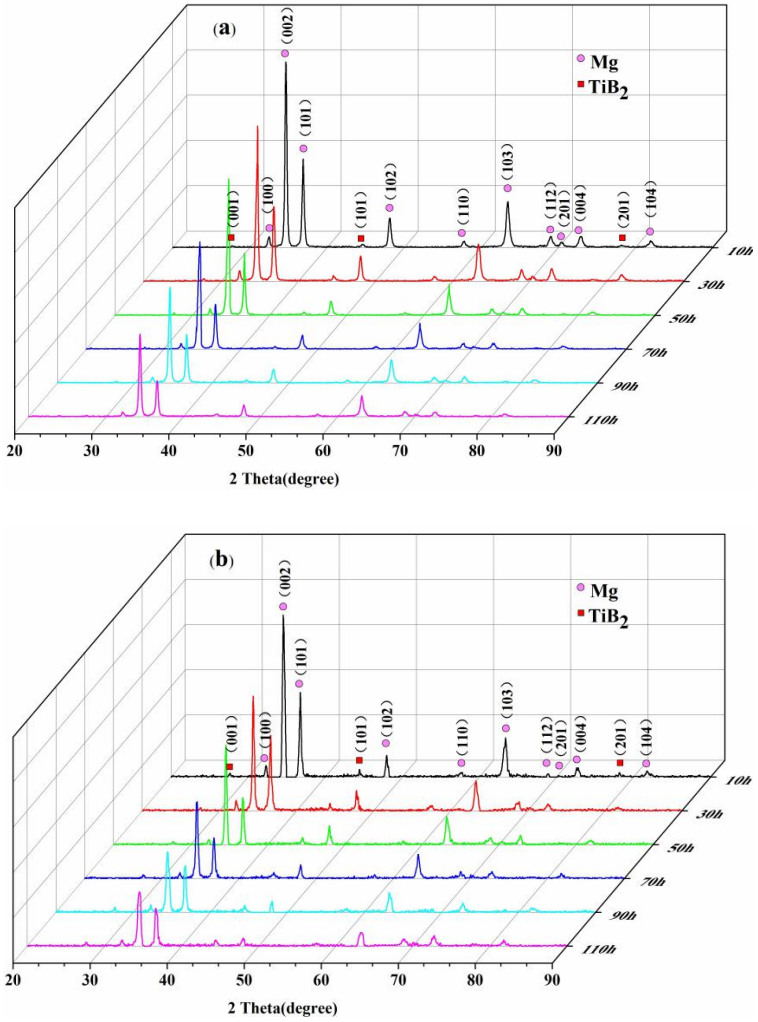

Figure 7. *Cont.*

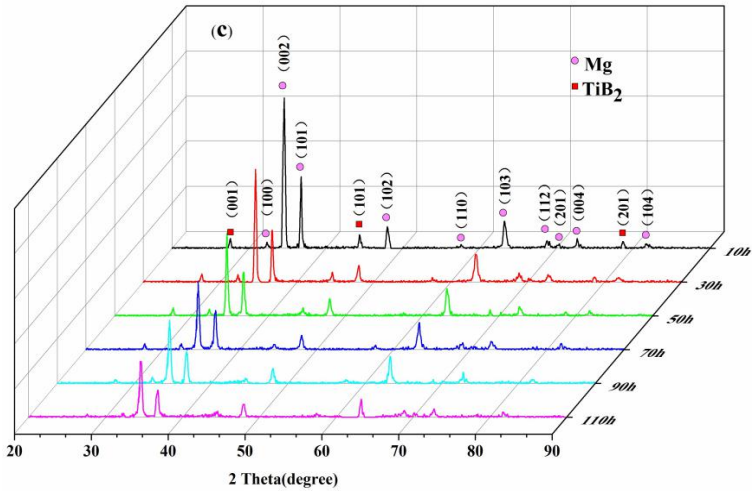

Figure 7. XRD patterns of AZ31/TiB_2 composite powders with different TiB_2 additions after milling for different times: (**a**) 2.5 wt %, (**b**) 5 wt %, and (**c**) 10 wt %.

Figure 8 shows the grain size of the Mg matrix in milled composite materials, which was calculated by Equation (1). It can be observed that the grain size decreased with the increase of milling time, and there were three stages for the refinement of the grain size. In the initial milling stage, the grain refinement was rapid, and the grain size of the Mg matrix with different TiB_2 additions was refined to below 150 nm after milling for 50 h. During the initial milling stage, the composite powders suffered repeated plastic deformations with high strain rates, resulting in the increasing dislocation density. When the dislocation density reached a critical value, the grain broke up into sub-grains separated by low angle grain boundaries [31], leading to the rapid refinement of Mg grains. With further milling, the grain refining would promote the generation of a lot of new grain boundaries. As a result, the subsequent refining required a larger critical dislocation density and more energy. However, the input energy was constant during the milling process. Therefore, the grain refinement rate slowed down during the middle stage. It can be found that the grain size of the Mg matrix, with different TiB_2 additions, was refined to below 100 nm after milling for 70 h. In the last milling stage, the grain refinement rate decreased significantly, and reached a relatively stable stage. Such a phenomenon was mainly attributed to the dynamic balance between grain refinement and grain growth caused by the thermal effect. It should be noted that there was a temperature rise in the composite powders during the milling process, because of the intense impact between the grinding balls and the milling pots. Meanwhile, the temperature rise would provide favorable conditions for grain growth, and hinder grain refinement. After milling for 110 h, the grain sizes of the Mg matrices in the AZ31/TiB_2 composite powders with 2.5 wt %, 5 wt % and 10 wt % TiB_2 additions were refined to 58 nm, 39 nm and 27 nm, respectively.

From Figure 8, it also can be deduced that the grain refinement rate of the Mg matrix increased with the increasing TiB_2 additions. In other words, the grain refinement of the matrix during mechanical milling was accelerated by the TiB_2 additions. The pinning effect of TiB_2 particles can hinder the migration of grain boundaries and dislocations, which could inhibit the grain growth during the milling process. Besides that, the occurrence of TiB_2 particles could accelerate the dislocation pile-up. Thus, the dislocation density of the composite powders increased with the increasing TiB_2 additions, which could promote the grain refinement of the Mg matrix during the milling process.

Besides that, it is interesting to find that the TiB_2 peaks became weaker with the increasing milling time, and almost disappeared after 110 hours of milling, as shown in Figure 7. Such a phenomenon has also been recently observed in Cu-Ag alloys [32], steels [33] and doped ZnO [34], and it was closely related to grain boundary segregation effects. As mentioned in Figure 8, the Mg matrices were gradually refined to a nanocrystalline state with the increasing milling times, and contained a lot of

grain boundaries. The grain boundary segregation layers formed where the Ti and B atoms were hidden. In other words, the formation of grain boundary segregation layers led to weakened TiB_2 peaks during the mechanical milling.

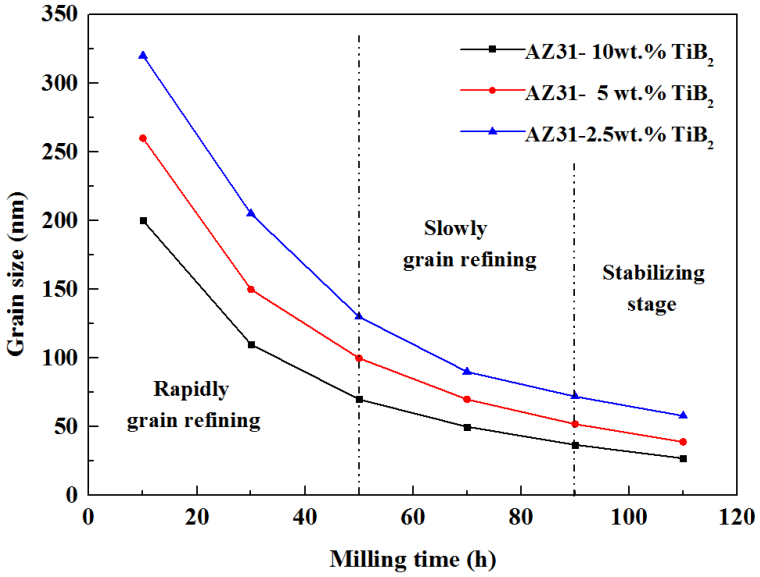

Figure 8. The grain size of the Mg matrix in the AZ31/TiB_2 composite powders, with different TiB_2 additions and after milling for different times.

3.4. TEM Analysis

As mentioned above, the milled AZ31/TiB_2 composite powders were cold pressed into green compacts, which were utilized for TEM observation. It should be noted that the TEM analysis could directly reveal the structure of nanocrystalline Mg matrices. Figure 8 shows the TEM images and corresponding grain size distributions of AZ31/TiB_2 composite powders, with different TiB_2 additions and after milling for 110 h. As shown in Figure 9a, it can be confirmed that the matrix phase was Mg by indexing the rings of the diffracted spots taken from the matrix grains. As shown in Figure 9b, the Mg matrix with 2.5 wt % TiB_2 particles had been refined to the nano-structure state after milling for 110 h, and most of the grains ranged from 31 to 79 nm. The average size of the Mg matrix was 53 nm, which was very close to the result calculated by Scherrer's formula (58 nm). With the increase of TiB_2 particles, the pinning effect of TiB_2 particles in the matrix was further enhanced, while the dislocation pile-up was also accelerated. As a result, the grain size was further refined with the increase of TiB_2 particles. From Figure 9c–f, it can be observed that the average sizes of the Mg matrices with 5 wt % and 10 wt % TiB_2 particles were refined to 37 nm and 23 nm, respectively. The average grain size values obtained from TEM observations were similar to the results calculated by Scherrer's formula, proving the validity of the former results.

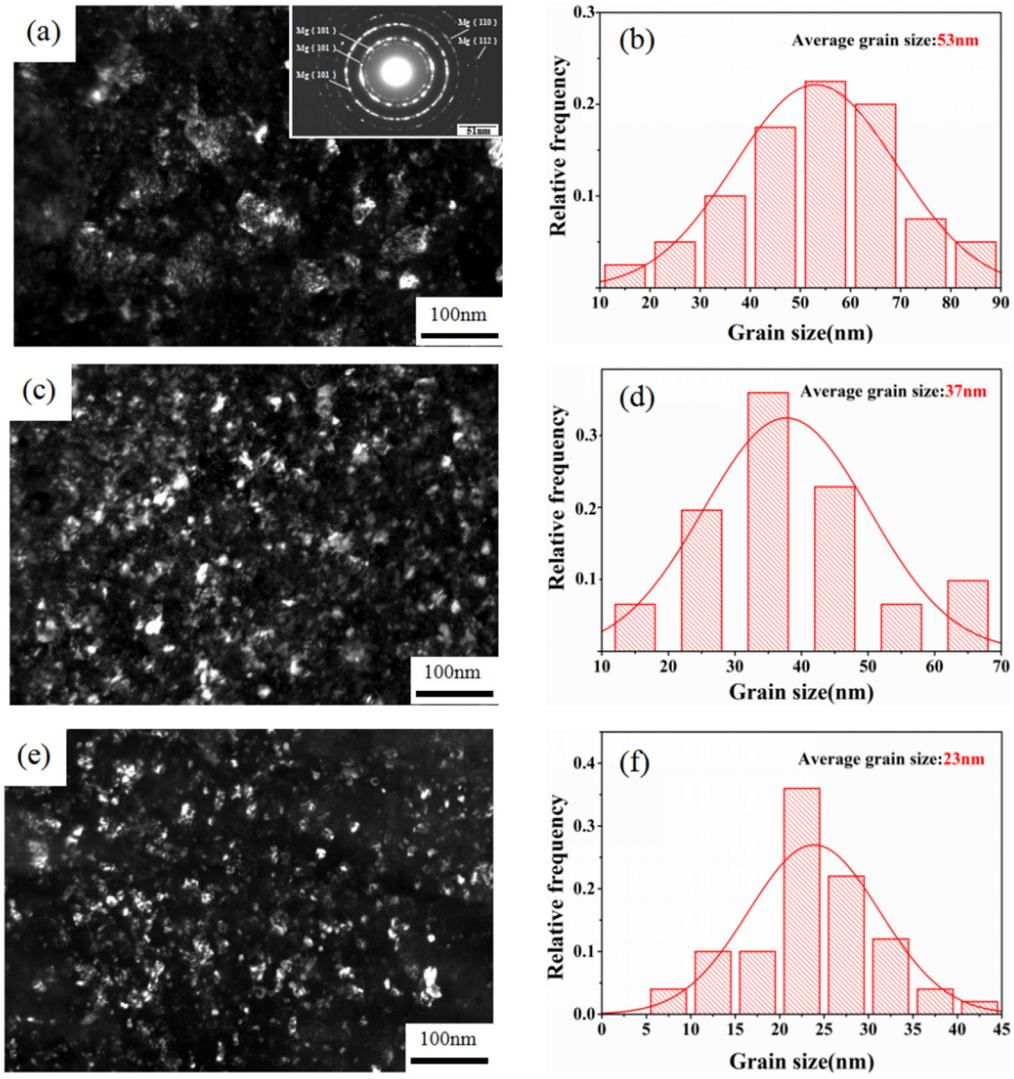

Figure 9. TEM images and corresponding grain size distributions of AZ31/TiB_2 composite powders with different TiB_2 additions after milling for 110 h: (**a**,**b**) 2.5 wt %, (**c**,**d**) 5 wt %, and (**e**,**f**) 10 wt %.

3.5. Hardness Analysis

The mechanical performance of the milled AZ31/TiB_2 composite powders was evaluated by micro-hardness testing. Figure 10 shows the micro-hardness of the as-cast AZ31 Mg alloy and as-milled AZ31/TiB_2 composites after milling for 110 h. It can be noted that the micro-hardness of the AZ31/TiB_2 composites was much greater than that of the as-cast AZ31 Mg alloy, which also increased with the increasing TiB_2 additions. For the AZ31–10 wt %TiB_2 composite, its micro-hardness was enhanced to 153 HV0.5. There were three main reasons for the significant increase in the micro-hardness of the AZ31/TiB_2 composites. The first one was grain boundary strengthening, which was closely related to the refinement of the Mg matrix. It has been reported that grain boundary strengthening can be calculated by the following formula [9,35,36]:

$$\Delta\sigma_{H-P} = k_\gamma d^{-\frac{1}{2}} \quad (2)$$

where k_γ is the Hall–Petch coefficient, and d is the mean grain size. After milling for 110 h, the grain size of the Mg matrix in the AZ31/TiB_2 composite powders was refined to nanocrystalline scale, and it was further refined with the increasing TiB_2 additions. The nanocrystalline matrix makes a great contribution to the improvement of micro-hardness. The second reason was the load-bearing effects

of submicron TiB_2 particles, which were much harder than the Mg matrix. The hard submicron TiB_2 particles would bear the load transferred from the Mg matrix, which could effectively enhance the micro-hardness of the composites. Meanwhile, it should be noticed that the load-bearing effects were improved with the increasing content of reinforcements [37]. In other words, the load-bearing effects of the AZ31/TiB_2 composites could be enhanced by increasing the TiB_2 additions. On the other hand, the submicron TiB_2 particles would give rise to Orowan strengthening, which was the third reason for the improvement of micro-hardness. The well-dispersed submicron TiB_2 particles could limit the migration of dislocations, and cause the remarkable strengthening.

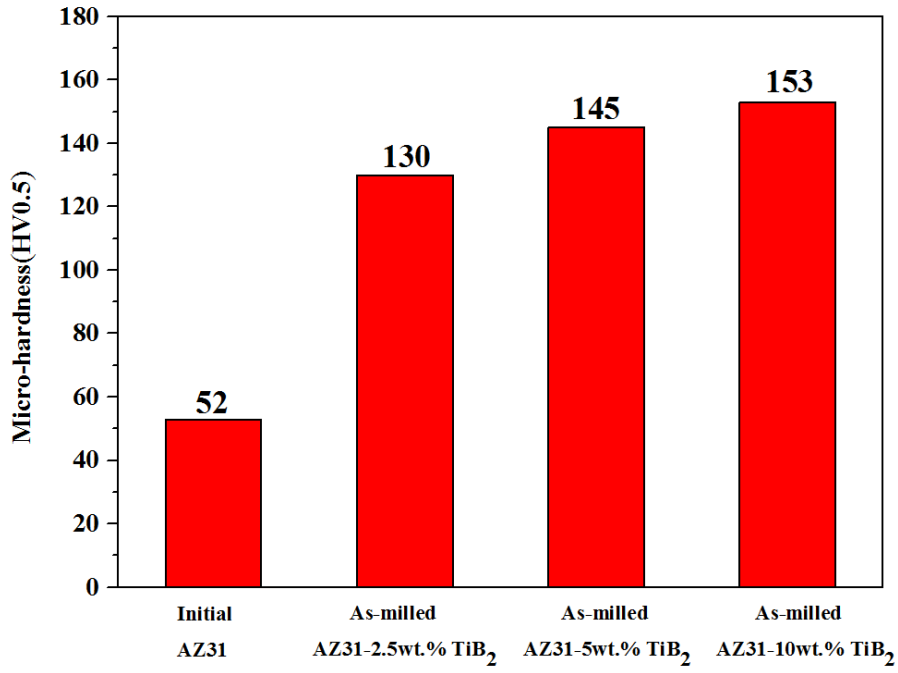

Figure 10. The Vickers micro-hardness of the as-cast AZ31 Mg alloy and as-milled AZ31/TiB_2 composites after milling for 110 h.

A comparison of the micro-hardness and grain sizes of various Mg alloys was carried out, as shown in Figure 11. The preparation processing included high-pressure torsion (HPT), spray-formed processing (SFP), disintegrated melt deposition (DMD), extrusion (ES), friction stir processing (FSP) and mechanical milling (MM). As can be concluded by the data comparison, the AZ31–10 wt % TiB_2 composite in this study exhibited a competitive micro-hardness among the other Mg alloys that have been referred to, and it possessed the smallest grain size. The nanocrystalline matrix and the well-dispersed submicron TiB_2 particles made great contributions to the mechanical performance of the AZ31/TiB_2 composite. From the comparison, it also can be concluded that MM was a feasible process for preparing TiB_2 particles to reinforce the Mg alloy with high micro-hardness.

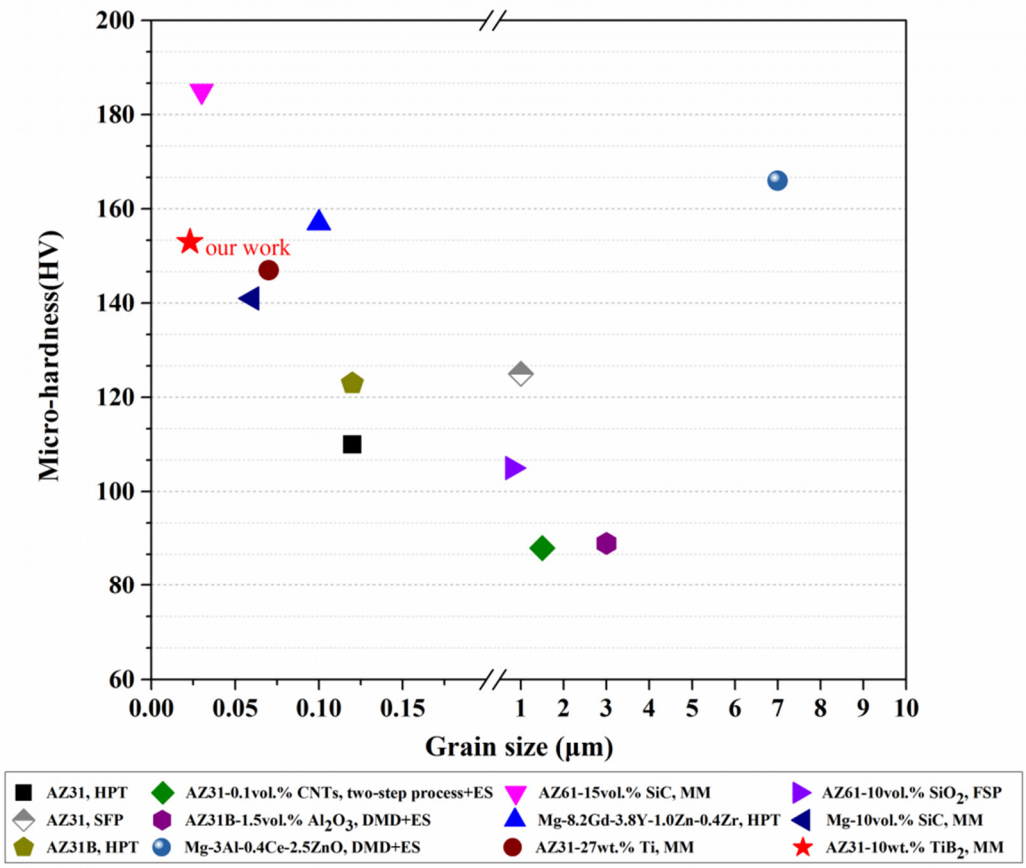

Figure 11. Comparison of the micro-hardness and grain sizes of various Mg alloys [25,38–47].

4. Conclusions

In this study, nanocrystalline AZ31 Mg alloy powders, reinforced with submicron TiB_2 particles, were prepared via mechanical milling. The microstructure evolution and properties of the composites were also investigated. The conclusions are as follows:

(1) TiB_2 particles stimulated the fracture and welding of the AZ31/TiB_2 powders, leading to the acceleration of the milling process. Meanwhile, TiB_2 particles were gradually refined and distributed in the Mg matrix with increasing milling times, while their sharp edges were also eliminated. After milling for 110 h, the average size of the TiB_2 particles in the AZ31–5 wt % TiB_2 composite was refined to about 0.4 μm, which had reached submicron scale.

(2) During the mechanical milling process, the matrix was significantly refined, and it was also accelerated by the TiB_2 particles. The grain sizes of AZ31–2.5 wt % TiB_2, AZ31–5 wt % TiB_2 and AZ31–10 wt % TiB_2 powders were refined to 53 nm, 37 nm and 23 nm, after milling for 110 h. In addition, the formation of grain boundary segregation layers led to the weakened TiB_2 peaks in the XRD patterns during mechanical milling.

(3) Under the combined effect of the nanocrystalline matrix and the well-dispersed submicron TiB_2 particles, the AZ31/TiB_2 composites exhibited greater micro-hardness, and the micro-hardness of the AZ31–10 wt % TiB_2 composite reached 153 HV0.5. Meanwhile, the micro-hardness of the AZ31/TiB_2 composites also increased with increasing TiB_2 additions.

Author Contributions: Investigation, H.Z. (Haiping Zhou), C.Z., J.Q., S.Q., K.G., J.L., S.S., H.Z. (Hongbin Zhang); resources, B.H., J.Q.; writing—original draft preparation, H.Z. (Haiping Zhou), H.Z. (Hongbin Zhang); writing—review and editing, H.Z. (Hongbin Zhang), C.Z.; project administration, J.Q.; funding acquisition, H.Z. (Haiping Zhou), J.Q., K.G., H.Z. (Hongbin Zhang). All authors have read and agreed to the published version of the manuscript.

Funding: This work has been supported by the National Natural Science Foundation of China (No. 51804187 and 51904176), Natural Science Foundation of Shandong Province (No. ZR2018BEE007), Project funded by China Postdoctoral Science Foundation (No. 2019M662400), Project of Shandong Province Higher Educational Young Innovative Talent Introduction and Cultivation Team [Performance enhancement of deep coal mining equipment], and Taishan Scholars Program of Shandong Province (No. TS201712065).

Conflicts of Interest: The authors declare no conflict of interest. All the funders played roles in the design of the study; in the collection, analyses of data and in the writing of the manuscript.

References

1. Suryanarayana, C.; Al-Aqeeli, N. Mechanically alloyed nanocomposites. *Prog. Mater. Sci.* **2013**, *58*, 383–502. [CrossRef]
2. Feng, J.; Sun, H.; Li, X.; Zhang, J.; Fang, W.; Fang, W. Microstructures and mechanical properties of the ultrafine-grained Mg–3Al–Zn alloys fabricated by powder metallurgy. *Adv. Powder Technol.* **2016**, *27*, 550–556. [CrossRef]
3. Pourbahari, B.; Emamy, M.; Mirzadeh, H. Synergistic effect of Al and Gd on enhancement of mechanical properties of magnesium alloys. *Prog. Nat. Sci. Mater. Int.* **2017**, *27*, 228–235. [CrossRef]
4. Asgharzadeh, H.; Yoon, E.Y.; Chae, H.J.; Kim, T.S.; Lee, J.W.; Kim, H.S. Microstructure and mechanical properties of a Mg–Zn–Y alloy produced by a powder metallurgy route. *J. Alloys Compd.* **2014**, *586*, S95–S100. [CrossRef]
5. Hofstetter, J.; Rüedi, S.; Baumgartner, I.; Kilian, H.; Mingler, B.; Povoden-Karadeniz, E.; Pogatscher, S.; Uggowitzer, P.J.; Löffler, J.F. Processing and microstructure–property relations of high-strength low-alloy (HSLA) Mg–Zn–Ca alloys. *Acta Mater.* **2015**, *98*, 423–432. [CrossRef]
6. Yu, H.; Sun, Y.; Hu, L.; Zhou, H.; Wan, Z. Microstructural evolution of AZ61-10at.%Ti composite powders during mechanical milling. *Mater. Des.* **2016**, *104*, 265–275. [CrossRef]
7. Chaubey, A.K.; Scudino, S.; Khoshkhoo, M.S.; Prashanth, K.G.; Mukhopadhyay, N.K.; Mishra, B.K.; Eckert, J. High-strength ultrafine grain Mg–7.4%Al alloy synthesized by consolidation of mechanically alloyed powders. *J. Alloys Compd.* **2014**, *610*, 456–461. [CrossRef]
8. Shen, M.J.; Ying, W.F.; Wang, X.J.; Zhang, M.F.; Wu, K. Development of High Performance Magnesium Matrix Nanocomposites Using Nano-SiC Particulates as Reinforcement. *J. Mater. Eng. Perform.* **2015**, *24*, 3798–3807. [CrossRef]
9. Yuan, W.; Panigrahi, S.K.; Su, J.Q.; Mishra, R.S. Influence of grain size and texture on Hall–Petch relationship for a magnesium alloy. *Scr. Mater.* **2011**, *65*, 994–997. [CrossRef]
10. Stráská, J.; Janeček, M.; Gubicza, J.; Krajňák, T.; Yoon, E.Y.; Kim, H.S. Evolution of microstructure and hardness in AZ31 alloy processed by high pressure torsion. *Mater. Sci. Eng. A* **2015**, *625*, 98–106. [CrossRef]
11. Pérez-Prado, M.T.; Valle, d.; Ruano, O.A. Grain refinement of Mg–Al–Zn alloys via accumulative roll bonding. *Scr. Mater.* **2004**, *51*, 1093–1097. [CrossRef]
12. Gzyl, M.; Rosochowski, A.; Boczkal, S.; Olejnik, L. The role of microstructure and texture in controlling mechanical properties of AZ31B magnesium alloy processed by I-ECAP. *Mater. Sci. Eng. A* **2015**, *638*, 20–29. [CrossRef]
13. Chang, C.I.; Du, X.H.; Huang, J.C. Producing nanograined microstructure in Mg–Al–Zn alloy by two-step friction stir processing. *Scr. Mater.* **2008**, *59*, 356–359. [CrossRef]
14. Fang, W.-B.; Fang, W.; Sun, H.-F. Preparation of bulk ultrafine-grained Mg-3Al-Zn alloys by consolidation of ball milling nanocrystalline powders. *Trans. Nonferrous Metals Soc. China* **2011**, *21*, s247–s251. [CrossRef]
15. Suryanarayana, C. Mechanical alloying and milling. *Prog. Mater. Sci.* **2011**, *46*, 1–184. [CrossRef]
16. Matin, A.; Saniee, F.F.; Abedi, H.R. Microstructure and mechanical properties of Mg/SiC and AZ80/SiC nano-composites fabricated through stir casting method. *Mater. Sci. Eng. A* **2015**, *625*, 81–88. [CrossRef]
17. Aydin, F.; Sun, Y.; Ahlatci, H.; Turen, Y. Investigation of Microstructure, Mechanical and Wear Behaviour of B4C Particulate Reinforced Magnesium Matrix Composites by Powder Metallurgy. *Trans. Indian Inst. Metals* **2018**, *71*, 873–882. [CrossRef]
18. Su, H.; Gao, W.; Feng, Z.; Lu, Z. Processing, microstructure and tensile properties of nano-sized Al_2O_3 particle reinforced aluminum matrix composites. *Mater. Des.* **2012**, *36*, 590–596. [CrossRef]

19. Sankaranarayanan, S.; Habibi, M.K.; Jayalakshmi, S.; Ai, K.J.; Almajid, A.; Gupta, M. Nano-AlN particle reinforced Mg composites: Microstructural and mechanical properties. *Mater. Sci. Technol.* **2015**, *31*, 1122–1131. [CrossRef]
20. Rahmany-Gorji, R.; Alizadeh, A.; Jafari, H. Microstructure and mechanical properties of stir cast ZX51/Al2O3p magnesium matrix composites. *Mater. Sci. Eng. A* **2016**, *674*, 413–418. [CrossRef]
21. Wang, Y.; Wang, H.-Y.; Xiu, K.; Wang, H.-Y.; Jiang, Q.-C. Fabrication of TiB2 particulate reinforced magnesium matrix composites by two-step processing method. *Mater. Lett.* **2006**, *60*, 1533–1537. [CrossRef]
22. Xiao, P.; Gao, Y.; Xu, F.; Yang, S.; Li, B.; Li, Y.; Huang, Z.; Zheng, Q. An investigation on grain refinement mechanism of TiB2 particulate reinforced AZ91 composites and its effect on mechanical properties. *J. Alloys Compd.* **2019**, *780*, 237–244. [CrossRef]
23. Aydin, F.; Sun, Y. Investigation of wear behaviour and microstructure of hot-pressed TiB2 particulate-reinforced magnesium matrix composites. *Can. Metall. Q.* **2018**, *57*, 455–469. [CrossRef]
24. Lei, R.S.; Wang, M.P.; Li, Z.; Wei, H.G.; Yang, W.C.; Jia, Y.L.; Gong, S. Structure evolution and solid solubility extension of copper–niobium powders during mechanical alloying. *Mater. Sci. Eng. A* **2011**, *528*, 4475–4481. [CrossRef]
25. Zhou, H.; Hu, L.; Sun, Y.; Zhang, H.; Duan, C.; Yu, H. Synthesis of nanocrystalline AZ31 magnesium alloy with titanium addition by mechanical milling. *Mater. Charact.* **2016**, *113*, 108–116. [CrossRef]
26. Fogagnolo, J.B.; Velasco, F.; Robert, M.H.; Torralba, J.M. Effect of mechanical alloying on the morphology, microstructure and properties of aluminium matrix composite powders. *Mater. Sci. Eng. A* **2003**, *342*, 131–143. [CrossRef]
27. Bemanifar, S.; Rajabi, M.; Hosseinipour, S.J. Microstructural Characterization of Mg-SiC Nanocomposite Powders Fabricated by High Energy Mechanical Milling. *Silicon* **2017**, *9*, 823–827. [CrossRef]
28. Hesabi, Z.R.; Simchi, A.; Reihani, S.M.S. Structural evolution during mechanical milling of nanometric and micrometric Al2O3 reinforced Al matrix composites. *Mater. Sci. Eng. A* **2006**, *428*, 159–168. [CrossRef]
29. Slipenyuk, A.; Kuprin, V.; Milman, Y.; Goncharuk, V.; Eckert, J. Properties of P/M processed particle reinforced metal matrix composites specified by reinforcement concentration and matrix-to-reinforcement particle size ratio. *Acta Mater.* **2006**, *54*, 157–166. [CrossRef]
30. Zhang, S.L.; Zhao, Y.T.; Chen, G.; Cheng, X.N.; She, C.J.; Wang, X.Y.; Wu, D.N. Effects of in situ TiB2 particle on microstructures and mechanical properties of AZ91 alloy. *J. Alloys Compd.* **2010**, *494*, 94–97. [CrossRef]
31. Yu, H.; Sun, Y.; Hu, L.; Wan, Z.; Zhou, H. The effect of Ti addition on microstructure evolution of AZ61 Mg alloy during mechanical milling. *J. Alloys Compd.* **2017**, *704*, 537–544. [CrossRef]
32. Mazilkin, A.A.; Straumal, B.B.; Kilmametov, A.R.; Boll, T.; Baretzky, B.; Kogtenkova, O.A.; Korneva, A.; Zieba, P. Competition for impurity atoms between defects and solid solution during high pressure torsion. *Scr. Mater.* **2019**, *173*, 46–50. [CrossRef]
33. Ivanisenko, Y.; Sauvage, X.; Mazilkin, A.A.; Kilmametov, A.R.; Beach, J.A.; Straumal, B.B. Bulk Nanocrystalline Ferrite Stabilized through Grain Boundary Carbon Segregation. *Adv. Eng. Mater.* **2018**, *20*, 1800443. [CrossRef]
34. Straumal, B.B.; Mazilkin, A.A.; Protasova, S.G.; Myatiev, A.A.; Straumal, P.B.; Baretzky, B. Increase of Co solubility with decreasing grain size in ZnO. *Acta Mater.* **2008**, *56*, 6246–6256. [CrossRef]
35. Su, S.; Zhou, J.; Tang, S.; Yu, H.; Su, Q.; Zhang, S. Synthesis of Nanocrystalline AZ91 Magnesium Alloy Dispersed with 15 vol.% Submicron SiC Particles by Mechanical Milling. *Materials* **2019**, *12*, 901. [CrossRef]
36. Schuh, C.A.; Nieh, T.G.; Iwasaki, H. The effect of solid solution W additions on the mechanical properties of nanocrystalline Ni. *Acta Mater.* **2003**, *51*, 431–443. [CrossRef]
37. Goh, C.S.; Wei, J.; Lee, L.C.; Gupta, M. Properties and deformation behaviour of Mg–Y2O3 nanocomposites. *Acta Mater.* **2007**, *55*, 5115–5121. [CrossRef]
38. Silva, C.L.P.; Soares, R.B.; Pereira, P.H.R.; Figueiredo, R.B.; Lins, V.F.C.; Langdon, T.G. The Effect of High-Pressure Torsion on Microstructure, Hardness and Corrosion Behavior for Pure Magnesium and Different Magnesium Alloys. *Adv. Eng. Mater.* **2019**, *21*, 1801081. [CrossRef]
39. Saravanan, M.; Sivaiah, B.; Srivastava, A.K.; Dhar, A. Ultrafine grain structure features in spray-formed AZ31 magnesium alloy. *Mater. Des.* **2014**, *60*, 21–25. [CrossRef]
40. Chen, Q.; Shu, D.; Hu, C.; Zhao, Z.; Yuan, B. Grain refinement in an as-cast AZ61 magnesium alloy processed by multi-axial forging under the multitemperature processing procedure. *Mater. Sci. Eng. A* **2012**, *541*, 98–104. [CrossRef]

41. Shanthi, M.; Jayaramanavar, P.; Vyas, V.; Seenivasan, D.V.S.; Gupta, M. Effect of niobium particulate addition on the microstructure and mechanical properties of pure magnesium. *J. Alloys Compd.* **2012**, *513*, 202–207. [CrossRef]
42. Han, G.; Wang, Z.; Liu, K.; Li, S.; Du, X.; Du, W. Synthesis of CNT-reinforced AZ31 magnesium alloy composites with uniformly distributed CNTs. *Mater. Sci. Eng. A* **2015**, *628*, 350–357. [CrossRef]
43. Penther, D.; Ghasemi, A.; Riedel, R.; Fleck, C.; Kamrani, S. Effect of SiC nanoparticles on manufacturing process, microstructure and hardness of Mg-SiC nanocomposites produced by mechanical milling and hot extrusion. *Mater. Sci. Eng. A* **2018**, *738*, 264–272. [CrossRef]
44. Lee, C.J.; Huang, J.C.; Hsieh, P.J. Mg based nano-composites fabricated by friction stir processing. *Scr. Mater.* **2006**, *54*, 1415–1420. [CrossRef]
45. Nguyen, Q.B.; Gupta, M. Increasing significantly the failure strain and work of fracture of solidification processed AZ31B using nano-Al_2O_3 particulates. *J. Alloys Compd.* **2008**, *459*, 244–250. [CrossRef]
46. Seenuvasaperumal, P.; Doi, K.; Basha, D.A.; Singh, A.; Elayaperumal, A.; Tsuchiya, K. Wear behavior of HPT processed UFG AZ31B magnesium alloy. *Mater. Lett.* **2018**, *227*, 194–198. [CrossRef]
47. Li, R.; Xin, R.; Liu, Q.; Chapuis, A.; Liu, S.; Fu, G.; Zong, L. Effect of grain size, texture and density of precipitates on the hardness and tensile yield stress of Mg-14Gd-0.5Zr alloys. *Mater. Des.* **2017**, *114*, 450–458. [CrossRef]